ARMY RESEARCH LABORATORY

Self Assembled, Ultra-Hydrophobic Micro/Nano-Textured Surfaces

by Adam M. Rawlett, Joshua A. Orlicki, Nicole Zander, Afia Karikari, and Tim Long

ARL-TN-275 **April 2007**

NOTICES

Disclaimers

The findings in this report are not to be construed as an official Department of the Army position unless so designated by other authorized documents.

Citation of manufacturer's or trade names does not constitute an official endorsement or approval of the use thereof.

Destroy this report when it is no longer needed. Do not return it to the originator.

Army Research Laboratory
Aberdeen Proving Ground, MD 21005-5069

ARL-TN-275 **April 2007**

Self Assembled, Ultra-Hydrophobic Micro/Nano-Textured Surfaces

Adam M. Rawlett, Joshua A. Orlicki, and Nicole Zander
Weapons and Materials Research Directorate, ARL

Afia Karikari and Tim Long
Virginia Tech

REPORT DOCUMENTATION PAGE

Form Approved
OMB No. 0704-0188

1. REPORT DATE *(DD-MM-YYYY)*	2. REPORT TYPE	3. DATES COVERED (From - To)
April 2007	Final	October 2005–September 2006

4. TITLE AND SUBTITLE
Self Assembled, Ultra-Hydrophobic Micro/Nano-Textured Surfaces

5a. CONTRACT NUMBER

5b. GRANT NUMBER

5c. PROGRAM ELEMENT NUMBER

6. AUTHOR(S)
Adam M. Rawlett, Joshua A. Orlicki, Nicole Zander, Afia Karikari,* and Tim Long*

5d. PROJECT NUMBER
AH84

5e. TASK NUMBER

5f. WORK UNIT NUMBER

7. PERFORMING ORGANIZATION NAME(S) AND ADDRESS(ES)
U.S. Army Research Laboratory
ATTN: AMSRD-ARL-WM-MA
Aberdeen Proving Ground, MD 21005-5069

8. PERFORMING ORGANIZATION REPORT NUMBER
ARL-TN-275

9. SPONSORING/MONITORING AGENCY NAME(S) AND ADDRESS(ES)

10. SPONSOR/MONITOR'S ACRONYM(S)

11. SPONSOR/MONITOR'S REPORT NUMBER(S)

12. DISTRIBUTION/AVAILABILITY STATEMENT
Approved for public release; distribution is unlimited.

13. SUPPLEMENTARY NOTES
*Virginia Tech University, Department of Chemistry, Blacksburg, VA 24060

14. ABSTRACT
The formation of hierarchically ordered arrays of spherical cavities on polymer films is of interest due to potential applications in the preparation of photonic bandgaps materials, environmental sensors, and patterned light-emitting diodes. While many methods are known for the preparation of these porous materials, the breath figure approach has received significant scrutiny because of the simple and robust mechanism of pattern formation. Breath figures are patterned arrays of micrometer-sized defects in a polymer film, formed when water droplets condense onto a polymer solution surface during film drying. By controlling variables such as relative humidity and solvent, the feature size and uniformity of the resultant pattern can be controlled. The breath figure approach is valuable because it is versatile, inexpensive, and provides the advantages of large area ordering in the nano and micrometer regime.
The self assembly of regular arrays of nano and microscale pores in polymer matrices generated using the breath figure technique is being explored. Experimental parameters are modified to vary the size, spacing, organization, and long-range order of these self-organizing surfaces. Utilizing these regular arrays of pores as templates, we have patterned analogous arrays of pillars (inverse pores) from a polymer film cast onto the patterned surface. These micro/nano-textured surfaces have enhanced the hydrophobicity of the textured polymer when measured by contact angle. This method of producing ultra-hydrophobic textured surfaces should be amenable to high-throughput, low-cost manufacturing of myriad polymeric surfaces.

15. SUBJECT TERMS
self assembly, hydrophobic surfaces, breath figures, templating

16. SECURITY CLASSIFICATION OF:			17. LIMITATION OF ABSTRACT	18. NUMBER OF PAGES	19a. NAME OF RESPONSIBLE PERSON
a. REPORT	b. ABSTRACT	c. THIS PAGE			Adam M. Rawlett
UNCLASSIFIED	UNCLASSIFIED	UNCLASSIFIED	UL	24	19b. TELEPHONE NUMBER (*Include area code*) 410-306-0695

Standard Form 298 (Rev. 8/98)
Prescribed by ANSI Std. Z39.18

Contents

List of Figures iv

List of Tables v

Acknowledgments vi

1. Background 1

2. Experimental Procedure 2

2.1 Materials and Instrumentation....2

2.2 Breath Figure Formation....2

2.3 Silicone Rubber Pillar Formation....3

3. Results and Discussion 3

3.1 Effect of Molecular Weight on Breath Figure Formation....3

3.2 Effect of Concentration on Breath Figure Formation....7

3.3 Effect of Humidity Level on Breath Figure Formation....8

4. Templating From Breath Figures 8

5. Conclusions and Discussion 12

6. References 15

Distribution List 16

List of Figures

Figure 1. Schematic of breath figure formation (*6*). 1

Figure 2. Optical micrographs of variable molecular weight PS breath figures formed in CH_2Cl_2 (7 weight-percent) at 72% RH, clockwise from top left: 20-, 51-, and 160-kDa PS. 4

Figure 3. A series of confocal laser micrographs of PS 51 k breath figures formed in CH_2Cl_2 (7 weight-percent) at 73% RH. (A) Low magnification (10×, 921 × 921 μm at a wavelength of 458 nm), (B) medium magnification (20×, 461 × 461 μm at a wavelength of 633 nm), (C) high magnification (50×, 184 × 184 μm at a wavelength of 458 nm). 5

Figure 4. AFM images of different molecular weight PS breath figures formed in CH_2Cl_2 (7 weight-percent) at 72% RH. 5

Figure 5. Optical images of different molecular weight PS breath figures formed in CH_2Cl_2 (1 weight-percent) at 62% RH. Scale bar is 20 μm. 6

Figure 6. AFM images of PS (160 kg/mole) breath figures formed in CH_2Cl_2 at different concentrations and 72% RH. 7

Figure 7. Optical micrographs of PS breath figures (7 weight-percent) formed in CH_2Cl_2 at different humidity levels: (a) and (b) are 20- and 51-k PS formed at 68% RH respectively, while (c) and (d) are 20-k and 51-k formed at 72% RH, respectively. 9

Figure 8. Three-dimensional (3-D) AFM images of silicon pillars formed on breath figure template. In (a), the silicon rubber was crosslinked on a 51-k PS breath figure film formed in an uncontrolled environment, while for (b), it was crosslinked on a PS film of the same molecular formed in a humidity chamber at 73% RH. 10

Figure 9. AFM and optical images of silicone pillars (GE Silicones RTV 615 silicon rubber); (a) 3-D AFM image of the breath figure template before coating, (b) optical micrograph of the pillars, and (c) 3-D AFM image of the pillars. 10

Figure 10. AFM images of silicone pillars (Dow Corning 3120 RTV silicon rubber); (a) the breath figure template before coating, (b) optical micrograph of the pillars, and (c) atomic force micrograph of the pillars. 11

Figure 11. Typical defects observed in silicone pillar formation; (a) optical micrograph of a cluster of pillars, (b) the corresponding AFM image, and (c) AFM image obtained after pillars were improperly peeled. 12

Figure 12. Contact angle measurement (goniometer). Left: cured Si rubber (control) advancing CA = 100°, receding = 90°; right: cured Si rubber with pillars CA = 135°, receding = 127°. 12

Figure 13. A series of optical micrographs of monocarboxy terminated PS breath figures formed in CH_2Cl_2 (1 weight-percent) at 78% relative humidity. 13

Figure 14. Forward Fourier transformation of 1 weight-percent monocarboxy terminated PS. ..14

List of Tables

Table 1. Average diameter and depth of PS pores as a function of molecular weight at 72% RH measured via AFM. 6

Table 2. Average diameter and depth of PS pores as a function of molecular weight at 62% relative humidity measured by an optical microscope. 6

Table 3. Average diameter and depth of PS pores as a function of concentration at 72% RH measured by AFM. 8

Table 4. Average diameter and interval of 3 weight-percent 160-kDa PS pores as a function of humidity measured by an optical microscope. 9

Acknowledgments

The authors wish to thank Donovan Harris for his assistance and expertise in optical analysis and Mark VanLandingham for assistance with atomic force microscopy.

1. Background

The formation of hierarchically ordered arrays of spherical cavities on polymer films is of interest due to potential applications in the preparation of photonic bandgap materials, environmental sensors, and patterned light-emitting diodes (LED). While many methods are known for the preparation of these porous materials, the breath figure approach has received significant scrutiny because of the simple and robust mechanism of pattern formation (*1*, *2*). Breath figures are patterned arrays of micrometer-sized defects in a polymer film, formed when water droplets condensed onto a polymer solution surface during film drying. By controlling variables such as relative humidity (RH) and solvency, the feature size and uniformity of the resultant pattern can be controlled. The breath figure approach is valuable because it is versatile, inexpensive, and provides the advantages of large area ordering in the nano and micrometer regime.

The process is driven by the evaporation of an appropriate solvent under humid conditions, leading to a decrease in temperature at the air-liquid interface, resulting in water condensation (*3*). The drop-wise condensation proceeds according to several steps shown in figure 1. The first stage involves nucleation of the water droplets on the polymer solution surface. During the second stage, the droplets become larger and coalesce to minimize interfacial energy differences, resulting in pattern formation. With properly controlled conditions, a subsequent ordering of the droplets into a hexagonal lattice is observed (*4*). The temperature difference between the surface and the ambient conditions is minimized once the surface of the film is covered with water droplets. At this stage, the water droplets sink into the solution (depending upon solution density). Upon complete evaporation of the solvent, the pattern of the droplets generated in the polymer matrix is preserved as a hexagonally ordered array of pores with a honeycomb structure (*5*, *6*).

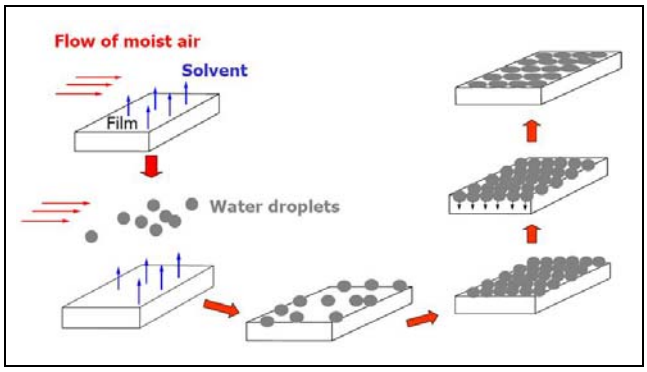

Figure 1. Schematic of breath figure formation (*6*).

The self assembly of regular arrays of nano and microscale pores in polymer matrices generated using the breath figure technique will be discussed. Experimental parameters to vary the size, spacing, organization, and long-range order of these self-organizing surfaces will also be discussed. Utilizing these regular arrays of pores as templates we have patterned analogous arrays of pillars (inverse pores) from a polymer film cast onto the patterned surface. These micro/nano-textured surfaces have enhanced the hydrophobicity of the textured polymer when measured by contact angle. This method of producing ultra-hydrophobic textured surfaces should be amenable to high-throughput, low-cost manufacturing of myriad polymeric surfaces.

2. Experimental Procedure

2.1 Materials and Instrumentation

Polystyrene with a series of molecular weights (M_n = 10, 19.8, 51, 97, 160, 411, and 670 kDa; polydispersity index [PDI] = 1.06 for all the polymers) were purchased from Pressure Chemical Company. In addition, monocarboxy and dicarboxy terminated polystyrenes with a series of molecular weights (M_n = 50, 100, 150, and 200 kDa) were purchased from Scientific Polymer Products. These materials were used to form the breath figure pores.

In order to prepare the array of pillars, two different silicone rubbers were evaluated. A high-viscosity, opaque rubber was obtained from Dow Corning 3120 RTV Silicone Rubber; GE Silicones provided a clear, low-viscosity resin, RTV615.

Atomic force microscopy (AFM) images were obtained on a Dimension 3100 AFM equipped with a Nanoscope* IV scanning probe microscope controller. Laser scanning confocal micrographs were taken with a Zeiss Pascal 5 confocal microscope equipped with two helium lasers and a multiwavelength Argon laser. Scanning electron microscopy (SEM) was performed using a Hitachi S-4700 instrument equipped with a field-emission cathode.

2.2 Breath Figure Formation

Two methods were utilized to form the breath figures. In the first setup, a humidity chamber was created using a plastic desiccator with a nitrogen inlet and outlet. To achieve an RH of 65%–80%, a saturated sodium chloride salt solution covered with parafilm† wrap was placed in the chamber at ambient temperature. A 20-mL disposable syringe barrel was inverted and used to bubble nitrogen gas through the saturated salt solution at a controlled rate. The RH was measured with a digital Dickson hygrometer and could be controlled by changing the gas velocity. The polymer solutions (1.0–10.0 weight-percent) were prepared by weighing

*Nanoscope is a registered trademark of Veeco Instruments, Inc., Camarillo, CA.

†Parafilm is a registered trademark of American Can Company, Greenwich, CT.

the required amount of polystyrene (PS) into a sample vial and dissolving it in dry CH_2Cl_2. The substrate, a DuPont Kapton* polyimide film (thickness 127 μm) was cut to the required size, rinsed twice with ethanol, and dried with nitrogen. The film was ozone treated for 20 s, taped to a standard glass microscope slide, and then placed in the humidity chamber. A 1.0 mL-drop of the PS solution was placed on the substrate in the humidity-controlled chamber, and the solvent was allowed to evaporate at room temperature at the required RH.

In the second setup, a Caron Environmental Chamber was used to electronically set the relative humidity, with the temperature kept near ambient conditions. For better adhesion, the glass microscope slide substrate was passed through a flame to burn off contaminants. The slides were then soaked for 1 hr in a 1% propyltrimethoxy silane solution in 90% (v/v) ethanol and water solution with a pH of 4.5. After rinsing with ethanol, the slides were dried at 70 °C. A 70-μL drop of the PS solution, prepared as previously described, was placed on the substrate in a mostly closed glass Petri dish in the chamber.

2.3 Silicone Rubber Pillar Formation

In order to prepare the array of pillars, two different silicone rubbers were evaluated. Both systems required the mixing of a 10:1 mixture of silicone rubber pre-polymer and catalyst. After thorough mixing, the resin was degassed under vacuum for 20 min. The silicone resin was then coated via pipette on the PS breath figures. The samples were subsequently cured in an oven at 60 °C for 16 hr. Selected samples were post-cured at 120–130 °C for 4 hr. After curing, the samples were cooled to room temperature and then cut into two equal portions. One sample was developed (removed from the PS breath figure substrate) by dissolution, the other by mechanical separation. For the dissolution route, tetrahydrofuran (THF) was used to selectively dissolve the PS breath figure leaving behind an array of pillars. The mechanical separation entailed the peeling-apart of the PS and silicone rubber films. While the mechanical method was faster, some level of surface damage was observed due to strong physisorption. For the monocarboxy and dicarboxy terminated PS, mechanical separation of the films was not possible due to the strong adhesion between the two polymers.

3. Results and Discussion

3.1 Effect of Molecular Weight on Breath Figure Formation

A 7 weight-percent PS solution was prepared in CH_2Cl_2 for four different molecular weights: 10, 19.8, 51, and 160 kDa. A 1.0-mL drop of each solution was deposited on ozone-treated Kapton films in a humidity chamber at 72% relative humidity with constant nitrogen flow. The surface of the polymer solutions became turbid, indicating breath figure formation. Figure 2

*Kapton is a registered trademark of DuPont Corporation, Newark, DE.

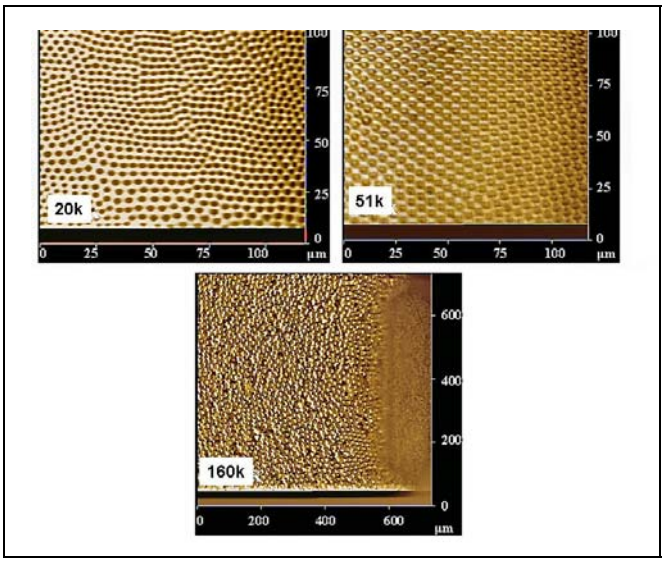

Figure 2. Optical micrographs of variable molecular weight PS breath figures formed in CH_2Cl_2 (7 weight-percent) at 72% RH, clockwise from top left: 20-, 51-, and 160-kDa PS.

shows the optical micrographs of the breath figures generated from various molecular weight PS solutions under the same conditions. The morphologies of the five films were significantly different, confirming molecular weight as a key parameter influencing pattern formation. For the 10-kDa film, the edges of the film scattered light (i.e., appeared turbid) while the central area remained clear. The optical micrograph for this film (not shown) established the presence of a few pores on the outskirts of the film and not on the remaining parts. In the case of the 20-kDa PS film, pores were observed uniformly across the surface but the order was confined to several small domains. Highly ordered pores were obtained for PS with a molecular weight of 51 kDa, as can be seen in figure 2 (center image). The pores in the 160-kDa film were disordered. Examination of the 51-kDa film using laser scanning confocal microscopy (figure 3) also confirmed the hexagonally packed, highly ordered honeycomb structures of the 51-kDa PS.

AFM images confirmed the optical microscope observations as shown in figure 4. The number-average diameter (D_n) and depth of the pores for the various molecular weights were determined by AFM and are summarized in table 1. Please note that depth and diameter measurements of the formed pores may be affected by the AFM tip geometry and will be further verified by confocal microscopy.

The effects of molecular weight variation were also examined in the Caron Humidity Chamber using 1 weight-percent solutions of polystyrene with weights of 19.8, 51, 97, 160, 411, and 670 kDa dissolved in CH_2Cl_2. A 70-µL drop of solution was placed on the silanized glass slide at 62% RH

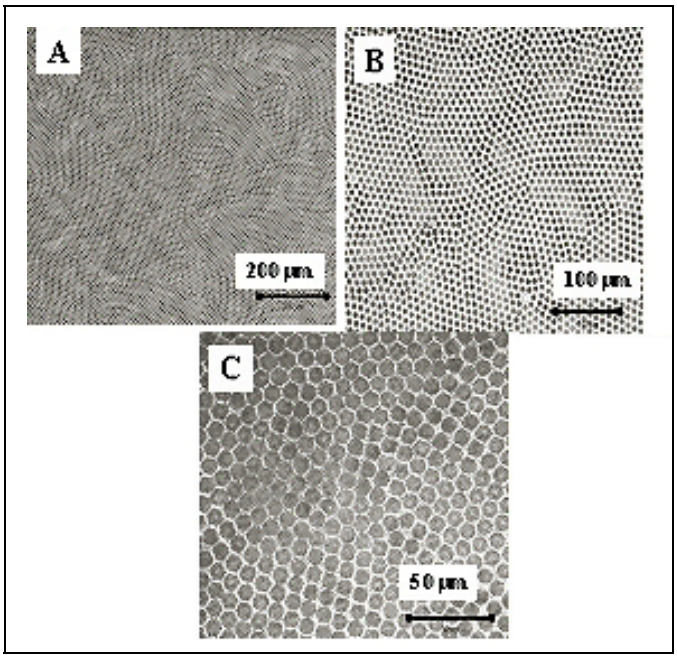

Figure 3. A series of confocal laser micrographs of PS 51 k breath figures formed in CH_2Cl_2 (7 weight-percent) at 73% RH. (A) Low magnification (10×, 921 × 921 µm at a wavelength of 458 nm), (B) medium magnification (20×, 461 × 461 µm at a wavelength of 633 nm), (C) high magnification (50×, 184 × 184 µm at a wavelength of 458 nm).

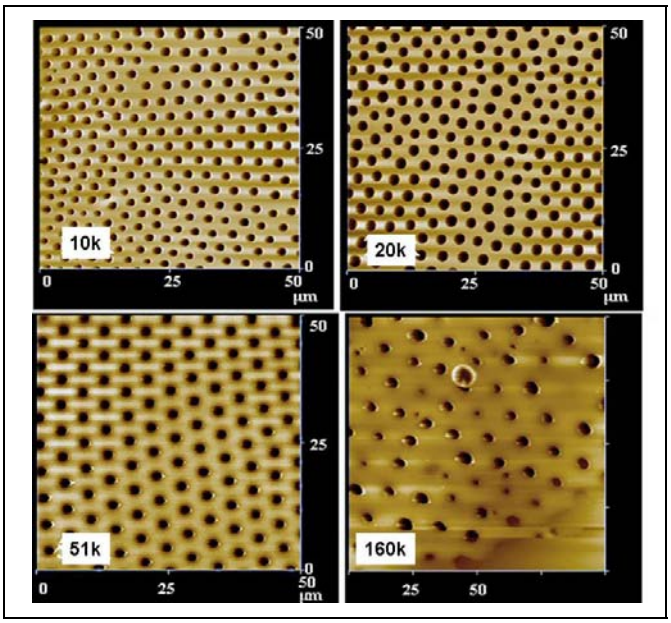

Figure 4. AFM images of different molecular weight PS breath figures formed in CH_2Cl_2 (7 weight-percent) at 72% RH.

Table 1. Average diameter and depth of PS pores as a function of molecular weight at 72% RH measured via AFM.

Molecular Weight (g/mole)	Diameter (μm)	Depth (μm)	Interval (μm)
10	2.3 ± 0.3	1.3 ± 0.2	1.2 ± 0.1
20	2.5 ± 0.2	2.2 ± 0.2	1.3 ± 0.1
51	3.4 ± 0.7	0.5 ± 0.1	1.6 ± 0.4
160	4.9 ± 1.2	1.2 ± 0.2	8.4 ± 1.4

and the solvent was allowed to evaporate. Table 2 shows the pore diameter and interval between pores. In this experiment, it was evident that increasing the molecular weight beyond 160 kDa yielded large gains in the pore size and spacing. Figure 5 displays optical images of select molecular weight PS. As the pore size increased for higher molecular weights, the array became more disordered.

Table 2. Average diameter and depth of PS pores as a function of molecular weight at 62% relative humidity measured by an optical microscope.

Molecular Weight (kDa)	Pore Diameter (μm)	Interval (μm)
19.8	4.3 ± 0.7	1.6 ± 0.3
51	4.1 ± 0.6	1.6 ± 0.6
97	2.4 ± 0.3	0.8 ± 0.3
160	4.2 ± 0.5	1.2 ± 0.4
411	11.8 ± 1.2	3.6 ± 0.7
670	13.4 ± 3.5	5.2 ± 1.4

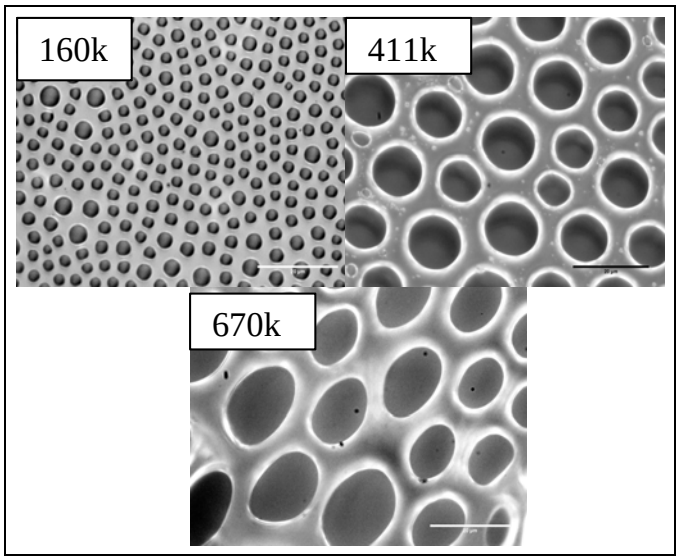

Figure 5. Optical images of different molecular weight PS breath figures formed in CH_2Cl_2 (1 weight-percent) at 62% RH. Scale bar is 20 μm.

The influence of molecular weight upon breath figure formation is related to the viscosity of the polymer in solution. A low-molecular-weight polymer exhibits a low-solution viscosity, permitting the coalescence of water droplets (*7*) by translational diffusion. This can result in disordered arrays of pores during breath figure formation. On the other hand, a very high-molecular-weight PS exhibits a high-solution viscosity; as such, the water droplets are not able to diffuse across the surface, leading to fewer pores in the films (figure 3). The results obtained for the 10-k film were different from those expected for a low molecular weight sample, as only a few ordered pores were observed. This result can be attributed to the use of CH_2Cl_2 in the film preparation, compared to $CHCl_3$ and toluene used in other published works (*7*). The higher vapor pressure of CH_2Cl_2 combined with the low molecular weight allowed for faster evaporation in the 10-k PS film. As a consequence, low overall viscosity of the 10-k sample resulted in preservation of the breath figure only at the edges that possess poor organization.

3.2 Effect of Concentration on Breath Figure Formation

As mentioned, the viscosity of the polymer solution plays an important role in the formation of regular breath figures. In this experiment, a series of PS solutions (160-k) ranging from 1 to 7 weight-percent were prepared and studied at 72% RH (figure 6). Highly ordered pores with monodisperse pore dimensions were observed for the 1 weight-percent PS film while the pores became more disorganized with increasing concentration. An increase in concentration was accompanied by an increase in pore-size polydispersity, leading to defects in the array formation (observed for the 7-weight-percent film in figure 6).

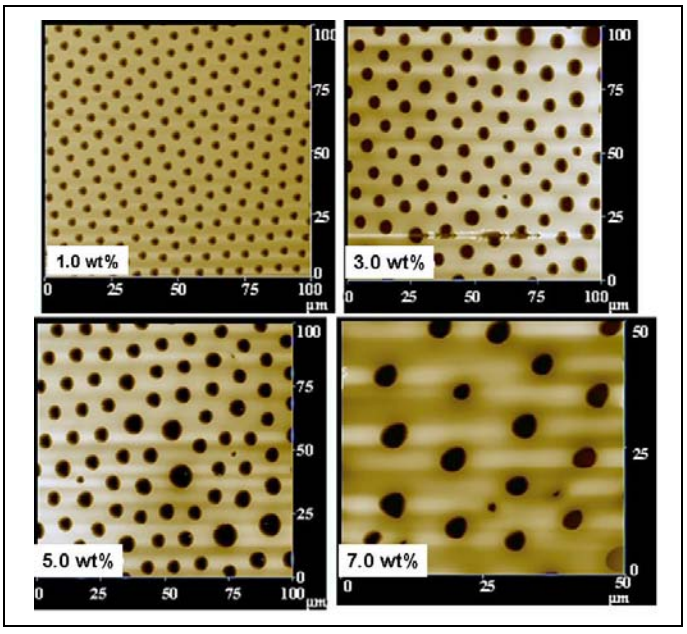

Figure 6. AFM images of PS (160 kg/mole) breath figures formed in CH_2Cl_2 at different concentrations and 72% RH.

From the summarized results in table 3, it is evident that the pore sizes became larger and more irregular as the concentration increased from 1 to 7 weight-percent. The average interval between adjacent pores was found to increase from 2.3 ± 0.4 to 9.5 ± 1.0 μm.

Table 3. Average diameter and depth of PS pores as a function of concentration at 72% RH measured by AFM.

Concentration (Weight-Percent)	Diameter (μm)	Depth (μm)	Interval (μm)
1.0	4.1 ± 0.3	3.1 ± 0.2	2.3 ± 0.4
3.0	6.0 ± 0.6	2.8 ± 0.5	5.0 ± 0.4
5.0	6.6 ± 0.7	4.1 ± 0.6	5.0 ± 0.9
7.0	5.9 ± 1.6	3.7 ± 0.8	9.5 ± 1.0

3.3 Effect of Humidity Level on Breath Figure Formation

In figure 7, the effect of humidity on breath figure formation in CH_2Cl_2 was studied for 20- and 51-k PS solutions at 68% and 72% RH. At 68% RH, highly disordered pores with several defects were observed in the 20-k PS film (figure 7a). For a 51-k solution under the same conditions, smaller pockets of ordered structures were obtained with a reduced number of defects as shown by the optical micrograph in figure 7b. An increase in the humidity level from 68% to 72% produced significant improvement of the morphology of two films as can be seen in figure 6c and figure 7d.

Complete suppression of the defects was observed. Increasing the humidity level directly increased the pore sizes. At low humidity levels (<40%), no breath figures are observed; at very high humidity levels (>90%), the rapidly condensing water droplets lead to coalescence of the droplets, subsequently resulting in disordered pattern formation and significant increases in the pore dimensions (*8*, *9*). Table 4 displays the results for a 3-weight-percent, 160-k PS solution in CH_2Cl_2. Although there was not strong correlation, the pore diameter, in general, increased with humidity.

4. Templating From Breath Figures

There has been an increase in the amount of research focused on the formation of organized arrays of silicon pillars (*10*). Tailored surface morphology allows control over wetting characteristics and optical appearance (e.g., matte vs. glossy). As an example, ultra-hydrophobic surfaces were developed from electron beam defined arrays of micron-sized pillars (*10*). Arrays of softer materials, such as high-aspect ratio polymer fibers, have been implemented in a biomimetic fashion to prepare non sticky adhesives, mimicking the morphology found on a gecko's foot pad (*11*, *12*).

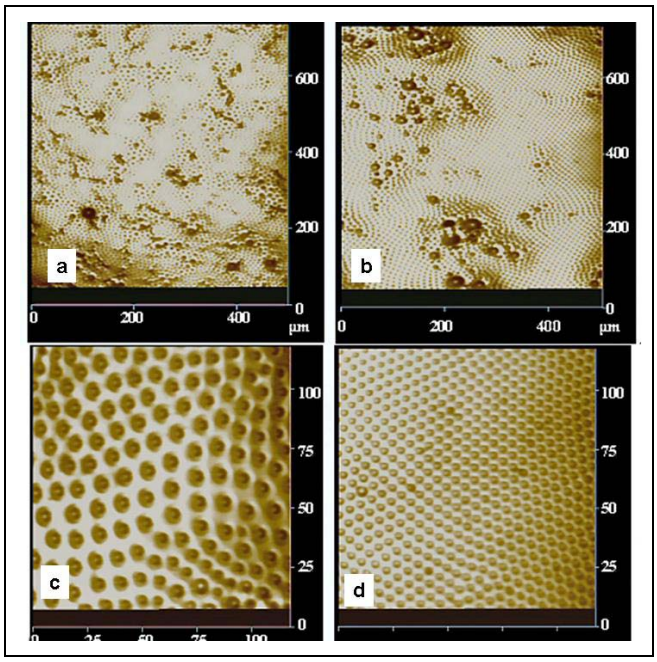

Figure 7. Optical micrographs of PS breath figures (7 weight-percent) formed in CH_2Cl_2 at different humidity levels: (a) and (b) are 20- and 51-k PS formed at 68% RH respectively, while (c) and (d) are 20-k and 51-k formed at 72% RH, respectively.

Table 4. Average diameter and interval of 3-weight-percent, 160-kDa PS pores as a function of humidity measured by an optical microscope.

Relative Humidity (%)	**Pore Diameter (µm)**	**Interval (µm)**
45	2.0 ± 0.5	2.2 ± 0.9
50	2.2 ± 0.2	1.7 ± 0.3
55	2.4 ± 0.2	2.0 ± 0.5
60	3.1 ± 0.7	2.3 ± 1.0
65	3.6 ± 0.4	2.4 ± 1.1
70	2.7 ± 0.5	1.6 ± 0.6
75	2.9 ± 0.4	1.2 ± 0.5
80	3.9 ± 0.7	2.1 ± 0.7
85	4.0 ± 0.9	2.2 ± 0.7
90	5.3 ± 1.0	2.6 ± 0.8

Breath figure arrays such as those described in the last section, were used as templates in an effort to generate micrometer-sized silicone rubber pillars, which may possess some properties analogous to those described above. The pillars were obtained by infiltrating the PS breath figures with two types of silicone rubber, crosslinking the rubber and then removing the PS

template by peeling the layers apart or by dissolving the PS in THF. Figure 8 depicts pillars formed by coating silicone rubber on disordered (a) and ordered (b) breath figure templates. The average diameter of the ordered array of pillars (figure 8b) was 4.5 ± 0.2 μm with a height of about 1.0 μm (removed by peeling).

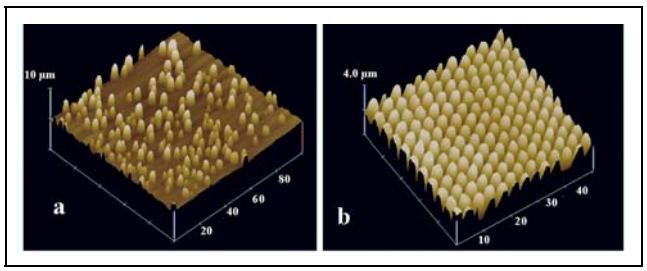

Figure 8. Three-dimensional (3-D) AFM images of silicon pillars formed on breath figure template. In (a), the silicon rubber was crosslinked on a 51-k PS breath figure film formed in an uncontrolled environment, while for (b), it was crosslinked on a PS film of the same molecular formed in a humidity chamber at 73% RH.

In figures 9 and 10, the AFM images of silicone pillars formed by coating the PS pores with a colorless low-viscosity rubber (GE Silicones RTV 615) (figure 9c) and a red, highly viscous (figure 10c) silicone rubber (Dow Corning 3120 RTV) are shown with the their corresponding breath figure templates and optical micrographs (removed by peeling).

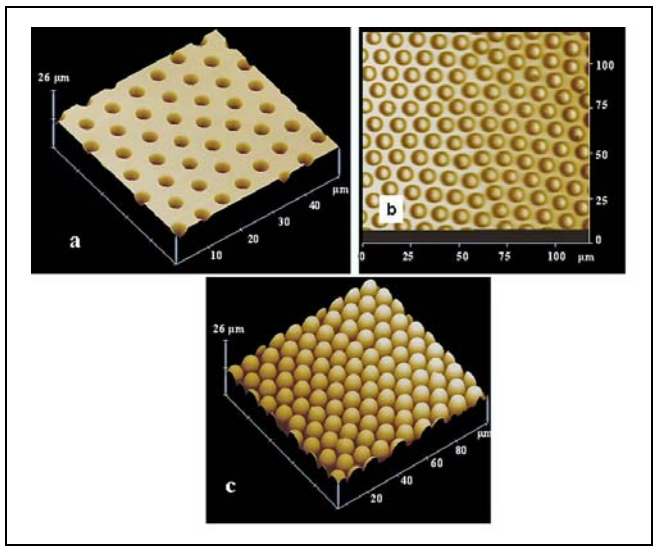

Figure 9. AFM and optical images of silicone pillars (GE Silicones RTV 615 silicon rubber); (a) 3-D AFM image of the breath figure template before coating, (b) optical micrograph of the pillars, and (c) 3-D AFM image of the pillars.

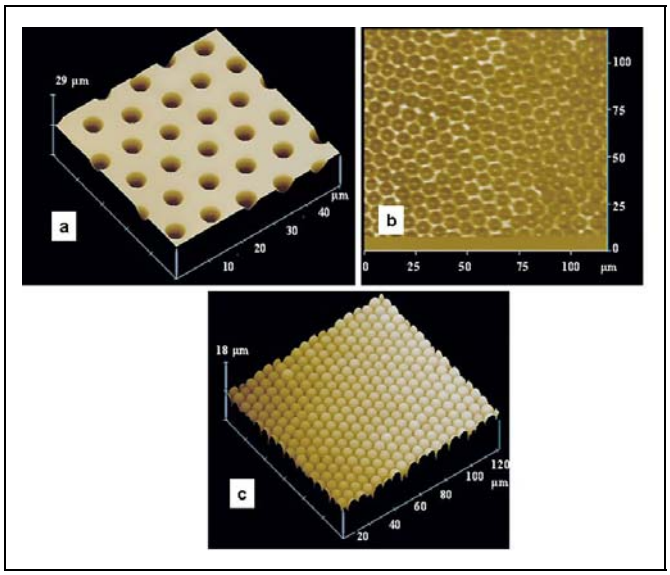

Figure 10. AFM images of silicone pillars (Dow Corning 3120 RTV silicon rubber); (a) the breath figure template before coating, (b) optical micrograph of the pillars, and (c) atomic force micrograph of the pillars.

In figure 9a, the average pore diameter and depth were 4.4 ± 0.1 µm and 3.0 ± 0.3 µm respectively. On the other hand, the corresponding pillar diameter and depth (figure 9c) were 10.6 ± 0.3 µm and 3.7 ± 0.4 µm, respectively. The increase in the pore dimensions can be attributed to swelling of the crosslinked pillars as a result of residual solvent since they were developed in THF and dried at 40 °C for 2 days. Similar results were obtained for the pillars formed with the highly viscous silicone rubber (figure 10).

The average pore diameter and depth (figure 10a) were 5.7 ± 0.2 µm and 3.5 ± 0.6 µm, respectively, while the pillar diameter and height were 6.5 ± 1.1 µm and 3.9 ± 0.6 µm, respectively.

Figure 11a and 11b show optical and AFM images of typical defects that were observed during the silicone pillar formation. These clusters of pillars were observed when the high-viscosity silicon rubber (Dow Corning 3120 RTV) was crosslinked without proper degassing. Such clusters were not observed with the low-viscosity rubber (GE Silicones RTV 615). In figure 11c, the AFM image of pillars that were obtained by improperly peeling off the PS template is shown. Red silicone rubber was observed on the PS template after peeling, signifying cohesive failure. Figure 12 demonstrates the effect of micro-patterning through breath figure templating on polymer surface morphology. This micro-texturing of the surface has enhanced the hydrophobicity of the polymer when measured by contact angle.

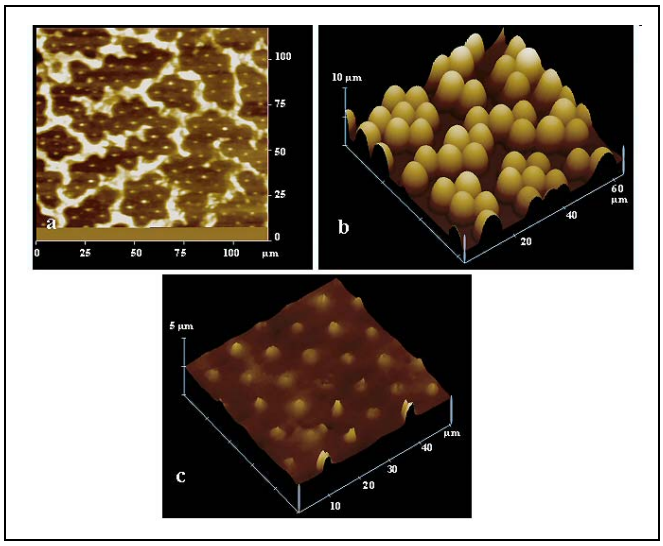

Figure 11. Typical defects observed in silicone pillar formation; (a) optical micrograph of a cluster of pillars, (b) the corresponding AFM image, and (c) AFM image obtained after pillars were improperly peeled.

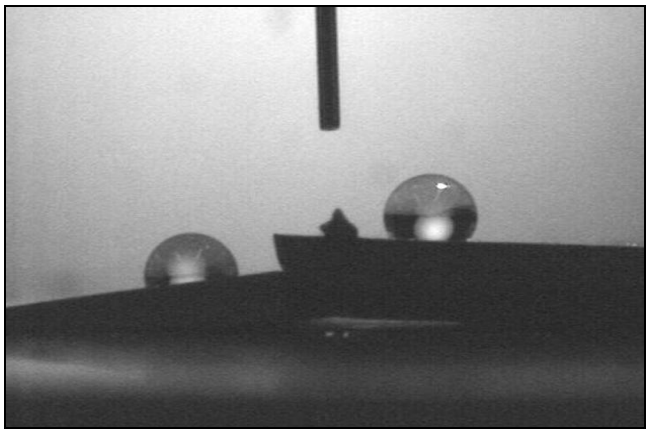

Figure 12. Contact angle measurement (goniometer). Left: cured Si rubber (control) advancing CA = 100°, receding = 90°; right: cured Si rubber with pillars CA = 135°, receding = 127°.

5. Conclusions and Discussion

Obtaining uniformly distributed arrays of pores was difficult to accomplish with the linear PS standards dissolved in an extremely volatile solvent (methylene chloride). The vapor pressure of

the solvent affects evaporation rate, and thus the rate of the breath figure formation. A fast evaporation induces a large perturbation of the system and the solvent can disappear before the drops form regular packing, resulting in defects in the array. Other less volatile solvents such as chloroform, benzene, and toluene were evaluated, but uniform breath figure formation was not observed. Casting a smaller droplet of solution in a mostly closed Petri dish slowed the evaporation rate and helped control the film thickness and uniformity.

In addition, monocarboxy and dicarboxy terminated polystyrenes were examined. These polymers, when dissolved in methylene chloride, gave much more reproducible films with uniformly patterned areas on the square-centimeter range. Magnifications of a 100-kDa monocarboxy terminated film are displayed in figure 13. Figure 14 shows a Fourier transformation of the breath figure array, and the hexagonal shape of the transform is indicative of the ordered packing of the breath figure structures.

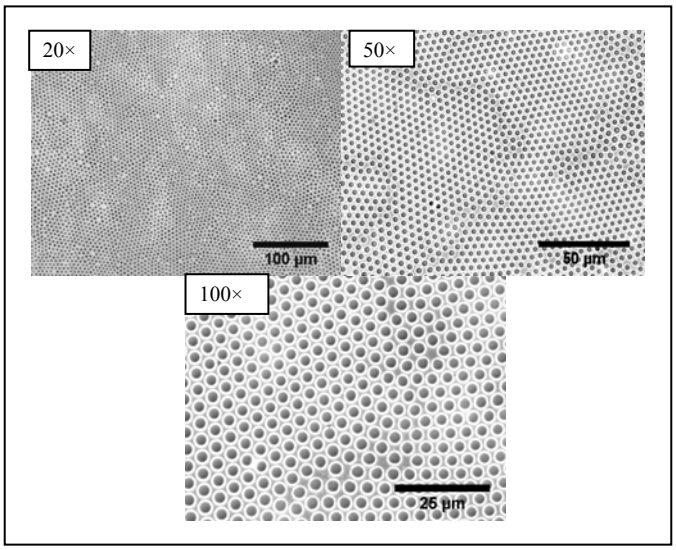

Figure 13. A series of optical micrographs of monocarboxy terminated PS breath figures formed in CH_2Cl_2 (1 weight-percent) at 78% relative humidity.

In summary, the effect of polymer molecular weight, solution viscosity, concentration, and relative humidity on the formation of ordered arrays of hexagonal pores were examined in CH_2Cl_2. Molecular weight was shown to strongly influence the formation of the ordered pores. PS with a low molecular weight (10 kDa) resulted in the formation of only a few pores while a high molecular weight resulted in the formation of disordered and highly polydispersed structures. Seven weight-percent solution concentrations led to the formation of disorganized and polydisperse pore sizes while highly ordered hexagonally packed monodisperse pores with large area ordering was observed for 1–3 weight-percent polystyrene solutions with a molecular weight of 160 kDa, as well as the mono and dicarboxy terminated polystyrenes. A linear

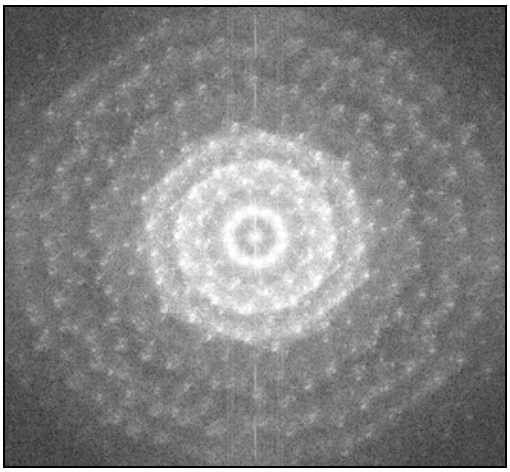

Figure 14. Forward Fourier transformation of 1 weight-percent monocarboxy terminated PS.

correlation was observed between humidity levels and the ordering of the pores. Highly ordered arrays of silicone rubber pillars were also obtained by using the PS breath figures as templates. These micro-textured surfaces greatly enhanced the hydrophobicity of the polymer when measured by contact angle. This method of producing ultra-hydrophobic textured surfaces should be amenable to high-throughput, low-cost manufacturing of myriad polymeric surfaces.

6. References

1. Yabu, H.; Shimomura, M. Simple Fabrication of Micro Lens Arrays. *Langmuir* **2005**, *21* (5), 1709–1711.

2. Englert, B. C.; Scholz, S.; Leech, P. J.; Srinivasarao, M.; Bunz, U. H. F. Templated Ceramic Microstructures by Using the Breath-Figure Method. *Chem. Eur. J.* **2005**, *11* (3), 995–1000.

3. Boker, A.; Lin, Y.; Chiapperini, K.; Horowitz, R.; Mark, T.; Carreeon, T. -X.; Abertz, C.; Skaff, H.; Dinsmore, A.; Emrick, T.; Russell, T. Hierarchical Nanoparticle Assemblies Formed by Decorating Breath Figures. *Nature Mater.* **2004**, *3*, 302–306.

4. Marcos-Martin, M.; Beysens, D.; Bouchaud, J. P.; Godreche, C.; Yekutieli, I. Self-Diffusion and 'Visited' Surface in the Droplet Condensation Problem (Breath Figures). *Physica A* **1995**, *214*, 396–412.

5. Park, M. S.; Kim, K. K. Breath Figure Patterns Prepared by Spin Coating in a Dry Environment. *Langmuir* **2004**, *20*, 5347–5352.

6. Mohan, S.; Collings, D.; Phillips, A.; Patel, S. Three-Dimensionally Ordered Array of Air Bubbles in a Polymer Film. *Science* **2001**, *292*, 79–83.

7. Peng, J.; Han, Y.; Yang, Y.; Binyao, L. The Influencing Factors on the Macroporous Formation in Polymer Films by Water Droplet Templating. *Polymer* **2004**, *45*, 447–452.

8. Gray, J. J.; Klein, D. H.; Korgel, B. A.; Bonnecaze, R. T. Microstructure Formation and Kinetics in the Random Sequential Adsorption of Polydisperse Tethered Nanoparticles Modeled as Hard Disks. *Langmuir* **2001**, *17*, 2317.

9. Steyer, A.; Guenoun, P.; Beysens, D.; Knobler, C. M. Two-Dimensional Ordering During Droplet Growth on a Liquid Surface . *Phys. Rev. B.* **1990**, *42*, 1086–1089.

10. Krupenkin, T. N.; Taylor, J. A.; Schneider, T. M.; Yang, S. From Rolling Ball to Complete Wetting: The Dynamic Tuning of Liquids on Nanostructured Surfaces. *Langmuir* **2004**, 20, 3824–3827.

11. Sitti, M.; Fearing, R. S. Synthetic Gecko Foot-Hair Science and Technology. *Journal of Adhesion Science and Technology* **2003**, *17* (8), 1055–1073.

12. Sitti, M.; Fearing, R. S. Micro/Nano-Structures as Dry Adhesives. *Journal of Adhesion Science and Technology* **2003**, *17* (8), 1055–1073.

NO. OF
COPIES ORGANIZATION

1 (PDF ONLY) DEFENSE TECHNICAL INFORMATION CTR
DTIC OCA
8725 JOHN J KINGMAN RD
STE 0944
FORT BELVOIR VA 22060-6218

1 US ARMY RSRCH DEV & ENGRG CMD
SYSTEMS OF SYSTEMS INTEGRATION
AMSRD SS T
6000 6TH ST STE 100
FORT BELVOIR VA 22060-5608

1 DIRECTOR
US ARMY RESEARCH LAB
IMNE ALC IMS
2800 POWDER MILL RD
ADELPHI MD 20783-1197

3 DIRECTOR
US ARMY RESEARCH LAB
AMSRD ARL CI OK TL
2800 POWDER MILL RD
ADELPHI MD 20783-1197

ABERDEEN PROVING GROUND

1 DIR USARL
AMSRD ARL CI OK TP (BLDG 4600)

NO. OF
COPIES ORGANIZATION

2 VIRGINIA TECH
DEPT OF CHEMISTRY
T LONG
BLACKSBURG VA 24060

2 VIRGINIA TECH
DEPT OF CHEMISTRY
A KARIKARI
BLACKSBURG VA 24060

ABERDEEN PROVING GROUND

10 DIR USARL
AMSRD ARL WM MA
A RAWLETT (2 CPS)
J ORLICKI (2 CPS)
N ZANDER (2 CPS)
M VANLANDINGHAM (2 CPS)
L GHIORSE (2 CPS)

INTENTIONALLY LEFT BLANK.